九州大学大学院総合理工学府報告
第 45 巻 第 2 号 1-10 頁 令和 6 年 2 月

Engineering Sciences Reports, Kyushu University
Vol. 45, No. 2, pp. 1-10, FEB, 2024

Emission Spectra of He_2* Excimer Produced from the $He_2^+/2e^-$ Collisional Radiative Recombination in the He Flowing Afterglow

Masaharu TSUJI*1,2† and Erika Oda−Sako*3
†E-mail of corresponding author: tsuji@cm.kyushu-u.ac.jp

(Received November 17, 2023, accepted December 1, 2023)

The $He_2^+/2e^-$ collisional radiative recombination (CRR) was studied by observing He_2* excimer emissions in the 200−990 nm region. He_2* emissions from twenty-two triplet states and twelve singlet states with excitation energies of 19.3−21.8 eV were identified. The relative formation rate constant of an upper u level of He_2*, $k_0(u)$, rapidly decreased with increasing the excitation energy of He_2*. Major triplet and singlet He_2* states were the lowest observed $c^3\Sigma_g^+$ and $C^1\Sigma_g^+$ states, which occupied 39.9% and 7.1% of $\sum_u k_0(u)$, respectively. The total formation ratio of triplet/singlet states was 5.1. No vibrational excitation was observed for all observed He_2* states. The rotational distributions of $f^3\Sigma_u^+(v'=0)$, $e^3\Pi_g(v'=0)$, and $c^3\Sigma_g^+(v'=0)$ were expressed by double Boltzmann rotational temperatures of 310–500 K and 580–990 K for low and high rotational levels, respectively, whereas that of $d^3\Sigma_u^+(v'=0)$ was expressed by a single Boltzmann rotational temperature of 650 K. Rovibrational distributions of the f, e, d, and C states indicated that most of the excess energies (95.2−98.5%) were deposited into relative translational energies of products. The observed vibrational and rotational distributions were lower than those of statistical prior ones calculated assuming a long lived [He_2*–e^-] intermediate.

Key words: *He_2^+ ion, Collisional radiative recombination, Flowing afterglow, He_2* excimer emission, Relative formation rate constant, Rotational temperature, Statistical prior distribution*

1. Introduction

There has been continuing interest in electron-ion recombination processes in discharge plasma because they are important loss processes of charged species from natural plasmas in space to man-made plasmas such as discharge plasma.[1,2] Since helium is an important rare gas for the formation of stable discharge plasma, electron-ion recombination processes in helium discharge plasma have been extensively studied.[3-9] The main purpose of previous experimental and theoretical studies has been the determination of the responsible recombination processes and their recombination coefficient or cross section at various electron densities, He pressures, and temperatures.

When the He gas pressure is low (p < about 1 Torr = 133.3 Pa), it is recognized that the three-body process $He^+ + 2e^- \rightarrow He^* + e^-$ is the main recombination mechanism if the electron density is not too low or the electron temperature too high. When the He gas pressure is higher (p > about 5 Torr) and He_2^+ is the dominant ion, the following electron-He_2^+ recombination processes can occur:

$He_2^+ + e^- \rightarrow$ neutral products,
Dissociation recombination (DR), (1)

$He_2^+ + e^- + e^- \rightarrow He_2^* + e^-$,
Collisional radiative recombination (CRR), (2)

$He_2^+ + e^- + He \rightarrow He_2^* + e^-$,
Ternary recombination. (3)

Berlande et al.[6] determined recombination coefficients of processes (1)–(3) at various electron densities and He pressures at 300 K. In general DR process (1) is slow and CRR process (2) is a major process at low He pressure and ternary recombination (3) becomes important with increasing the He gas pressure.

*1 Institute for Materials Chemistry and Engineering, and Research and Education Center of Green Technology
*2 Department of Molecular Science and Technology
*3 Department of Molecular Science and Technology, Graduate Student

Compared with the large number of kinetic studies of the He discharge plasma, there are only a few experimental studies on determining the final electronic states of neutral He_2 molecules in the electron-He_2^+ recombination process. Two pioneering flowing-afterglow (FA) optical spectroscopic studies have been carried out on the electron-He_2^+ recombination process leading to He_2^* excimer by Schmeltekopf and Broida[10] and Collins and Robertson[11] in 1963–1964. Schmeltekopf and Broida[10] observed several He_2^* emission systems resulting from CRR (2). Principal He_2^* emission systems were 4650 Å $e^3\Pi_g(3p\pi)$–$a^3\Sigma_u^+$ and 5733 Å $f^3\Delta_u(3d\delta)$–$b^3\Pi_g$ systems. They found that the rotational populations of high and low rotational levels of the $e^3\Pi_g$ state were expressed by double Boltzmann temperatures of 903 K and 492 K at p_{dn} (downstream pressure)[10] = 1.4 Torr and 878 and 278 K at p_{dn} = 1.7 Torr, respectively. Collins and Robertson[11] identified fourteen He_2^* bands with the wavelength near the band origin at 3680, 3984, 4400, 4430, 4450, 4540, 4650, 5130, 5730, 5880, 5950, 6100, 6300, and 6400 Å. Among fourteen emissions, five systems at 3680, 3984, 4450, 4650, and 5130 Å were assigned to the $4p\ ^3\Pi_g$–$2s\ ^3\Sigma_u^+$, $5d\ ^3\Pi_u$–$2p\ ^3\Pi_g$, $4d\ ^3\Sigma_u^+$–$2p\ ^3\Pi_g$, $3p\ ^3\Pi_g$–$2s\ ^3\Sigma_u^+$, and $3p\ ^1\Pi_g$–$2s\ ^1\Sigma_u^+$ transitions, respectively. Based on the axial variation and pressure dependence of the intensity of these He_2^* emissions and He_2^+ concentration, they identified the dominant populating mechanism of He_2^* to be CRR (2).[11] After these pioneering studies, no detailed optical studies have been reported for CRR process (2) during the past about 60 years.

We have previously made a systematic optical spectroscopic studies on the $He^+/2e^-$, $Ne^+/2e^-$, and $Ar^+/2e^-$ CRR reactions by observing He*, Ne*, and Ar* emissions in the FA.[12-15] In the $He^+/2e^-$ CRR reaction, the formation of fifty-one singlet and triplet *ns*, *np*, and *nd* Rydberg states of He* in the 23.01–24.53 eV range was observed. The electronic-state distribution decreased with increasing the excitation energy of He*. They were expressed by double Boltzmann electronic distributions with effective electronic temperatures of 0.46 eV in the 22.7–24.4 eV range and 0.089 eV in the 24.4–24.5 eV range.

In this study, the $He_2^+/2e^-$ CRR reaction (2) is investigated by observing ultraviolet-visible-near infrared emissions of He_2^* excimer in the He FA. The relative formation rate constants are determined. The vibrational and rotational distributions are determined and compared with those predicted from statistical prior distributions. Preliminary results of this paper were communicated in a review article.[16] Although the contribution of radiative cascade from upper He_2^* states to the lower levels was not considered in the determination of relative formation rate constant in the previous study,[16] we take it into account in this study.

2. Experimental

The FA apparatus used in this study has been previously described in detail.[16] In brief, the flow reactor, which consists of a quartz discharge tube (11 mm i. d.) and a stainless-steel reaction cell (60 mm i. d.), was continuously evacuated by means of a 10,000 liter/min mechanical booster pump combined with a 1,600 liter/min oil rotary pump. He(2^3S), He^+, He_2^+, electrons were generated by a microwave discharge of high purity helium gas (purity >99.995%) in a discharge flow operated at 1.6–20 Torr. The mechanical booster pump was equipped with a continuously variable gate valve.[16] Opening or closing the gate valve allowed us to vary the flow tube pressure from 1.8 Torr to 20 Torr. Low pressure experiments at 1.6–1.8 Torr were carried out by completely opening the gate valve, whereas high pressure experiments at 2–20 Torr were conducted by partially closing the gate valve.

The contribution of He^+ and He_2^+ ions to the observed emissions was examined using an ion-collector grid placed between the discharge section and the reaction zone. The efficiency of ion collection was found to be >98% by observing the $N_2^+(C^2\Sigma_u^+–X^2\Sigma_g^+)$ emission resulting from the $He^+ + N_2$ charge-transfer reaction.[17]

The positive He_2^+ ions were formed by the three-body reaction of He^+ with 2He in a flow tube:

$$He^+ + 2He \xrightarrow{k_4} He_2^+ + He, \quad (4)$$

($k_4 = 8.3 \times 10^{-32}$ cm^6 molecule^{-2} s^{-1} [Ref. 18]).

A reaction flame, observed 10 cm downstream from the center of the discharge, was dispersed in the 200–990 nm region with a Spex 1250M monochromator equipped with a cooled photomultiplier (Hamamatsu Photonics R376 or R316-02). The wavelength response of monochromator and the optical detection system were corrected using standard D_2 and halogen lamps.

3. Results and Discussion

3.1 Emission spectra of He_2* excimer resulting from the $He_2^+/2e^-$ CRR reaction

Figure 1 shows typical emission spectra observed in the 330−980 nm region at a He gas pressure of 1.8 Torr. Thirty triplet and twelve singlet transitions of He_2* given in Table 1 are identified by referring to reported molecular spectral data of He_2*.[19] The assignment of several weak transitions of He_2* is not shown in Fig. 1 for the sake of clarity. In addition to many He_2* emissions, He*, H*, and N_2^+(B−X) emissions are identified.[20,21] He* lines are dominantly formed by the $He^+/2e^-$ CRR reaction,[12,13] whereas H* lines and N_2^+ emission arise from residual H_2O and N_2, respectively.[21,22] The observed He_2* emissions disappeared when charged species were removed from the He afterglow on applying an electrostatic potential to the grid. These results imply that the He_2* states are produced through electron-ion recombination process.

The relative intensities of the observed He_2 transitions are listed in Table 1. There are

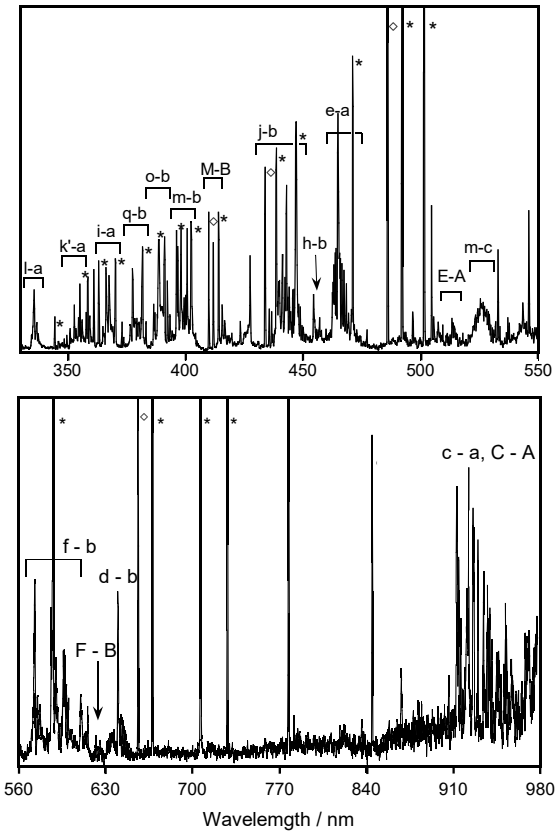

Fig. 1. Emission spectra of He_2* resulting from the $He_2^+/2e^-$ CRR in the He FA at a He gas pressure of 1.8 Torr. Lines marked by * and ◇ are He* and H* lines, respectively.

three $^3\Delta_u(n\mathrm{d}\delta)$, $^3\Pi_u(n\mathrm{d}\pi)$, and $^3\Sigma_u^+(n\mathrm{d}\sigma)$ components in the q, m, j, and f triplet states with n = 6, 5, 4, and 3, respectively. Although it was difficult to determine relative intensities of

Table 1. Relative intensities of He_2* excimer bands produced through the $He_2^+/2e^-$ CRR in the He FA.

Transition	RI[a)]	Transition	RI
$q^3\Delta_u(6d\delta)$-$b^3\Pi_g$	4.5		
$q^3\Pi_u(6d\pi)$-$b^3\Pi_g$			
$q^3\Sigma_u^+(6d\sigma)$-$b^3\Pi_g$			
$q^3\Delta_u(6d\delta)$-$c^3\Sigma_g^+$	1.9		
$q^3\Pi_u(6d\pi)$-$c^3\Sigma_g^+$			
$q^3\Sigma_u^+(6d\sigma)$-$c^3\Sigma_g^+$			
$p^3\Pi_g(6p\pi)$-$a^3\Sigma_u^+$	1.4	$P^1\Pi_g(6p\pi)$-$A^1\Sigma_u^+$	1.3
$o^3\Sigma_u^+(6s\sigma)$-$c^3\Sigma_g^+$	1.1		
$o^3\Sigma_u^+(6s\sigma)$-$b^3\Pi_g$	1.1		
$m^3\Delta_u(5d\delta)$-$c^3\Sigma_g^+$	3.0		
$m^3\Pi_u(5d\pi)$-$c^3\Sigma_g^+$			
$m^3\Sigma_u^+(5d\sigma)$-$c^3\Sigma_g^+$			
$m^3\Delta_u(5d\delta)$-$b^3\Pi_g$	5.6	$M^1\Delta_u(5d\delta)$-$B^1\Pi_g$	1.0
$m^3\Pi_u(5d\pi)$-$b^3\Pi_g$		$M^1\Pi_u(5d\pi)$-$B^1\Pi_g$	
$m^3\Sigma_u^+(5d\sigma)$-$b^3\Pi_g$		$M^1\Sigma_u^+(5d\sigma)$-$B^1\Pi_g$	
$l^3\Pi_g(5p\pi)$-$a^3\Sigma_u^+$	3.6	$L^1\Pi_g(5p\pi)$-$A^1\Sigma_u^+$	2.4
$k^3\Sigma_u^+(5s\sigma)$-$c^3\Sigma_g^+$	1.3		
$k^3\Sigma_u^+(5s\sigma)$-$b^3\Pi_g$	1.5		
$k'^3\Sigma_g^+(5p\sigma)$-$a^3\Sigma_u^+$	1.2		
$j^3\Delta_u(4d\delta)$-$b^3\Pi_g$	17.0		
$j^3\Pi_u(4d\pi)$-$b^3\Pi_g$			
$j^3\Sigma_u^+(4d\sigma)$-$b^3\Pi_g$			
$i^3\Pi_g(4p\pi)$-$a^3\Sigma_u^+$	6.3		
$h^3\Sigma_u^+(4s\sigma)$-$b^3\Pi_g$	2.2	$H^1\Sigma_u^+(4s\sigma)$-$B^1\Pi_g$	1.3
$f^3\Delta_u(3d\delta)$-$b^3\Pi_g$	14.1	$F^1\Delta_u(3d\delta)$-$B^1\Pi_g$	3.4
$f^3\Pi_u(3d\pi)$-$b^3\Pi_g$	15.0	$F^1\Pi_u(3d\pi)$-$B^1\Pi_g$	3.1
$f^3\Sigma_u^+(3d\sigma)$-$b^3\Pi_g$	11.9	$F^1\Sigma_u^+(3d\sigma)$-$B^1\Pi_g$	1.9
$e^3\Pi_g(3p\pi)$-$a^3\Sigma_u^+$	10.5	$E^1\Pi_g(3p\pi)$-$A^1\Sigma_u^+$	1.9
$d^3\Sigma_u^+(3s\sigma)$-$b^3\Pi_g$	13.2	$D^1\Sigma_u^+(3s\sigma)$-$B^1\Pi_g$	4.6
$c^3\Sigma_g^+(3p\sigma)$-$a^3\Sigma_u^+$	100	$C^1\Sigma_g^+(3p\sigma)$-$A^1\Sigma_u^+$	17.7

a) Relative intensity

the three components for the upper q, m, and j states because of their heavy overlapping in the narrow wavelength region. Therefore, total intensities of the three components in each system are given in Table 1. On the other hand, three components were observed separately for the f state, so that their relative intensities are given in Table 1.

Figures 2 and 3 show energy-level diagrams of triplet and singlet states of He_2^*, where observed emitting levels are shown in red. The excitation energies of He_2^* and the recombination energy of He_2^+ (22.223 eV) were obtained from Ref. 19. Although all of the He_2^* states below the recombination energy of He_2^+ can be formed in the $He_2^+/2e^-$ CRR reaction, 22 triplet levels from c to q states in the 19.2–21.9 eV region and 12 singlet levels from C to P states in the 19.5–21.8 eV region were observed in this study. These results indicate that product He_2^* are distributed in a wide energy range in both triplet and singlet states. A similar wide product-state distribution has been observed in the formation of He* from the $He^+/2e^-$ CRR reaction.[13)]

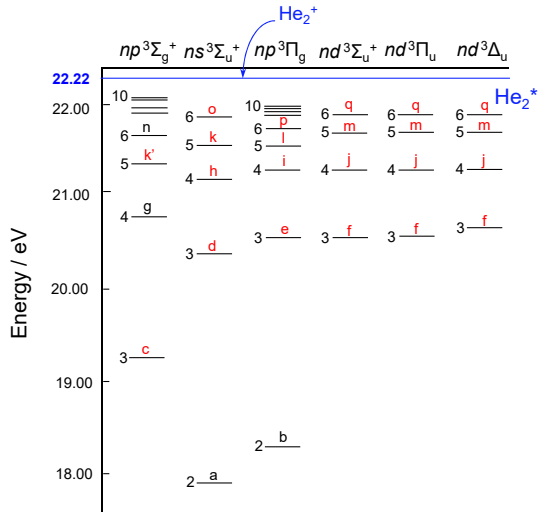

Fig. 2. Energy-level diagram of triplet states of He_2^*. Observed emitting levels in the $He_2^+/2e^-$ CRR reaction are shown in red.

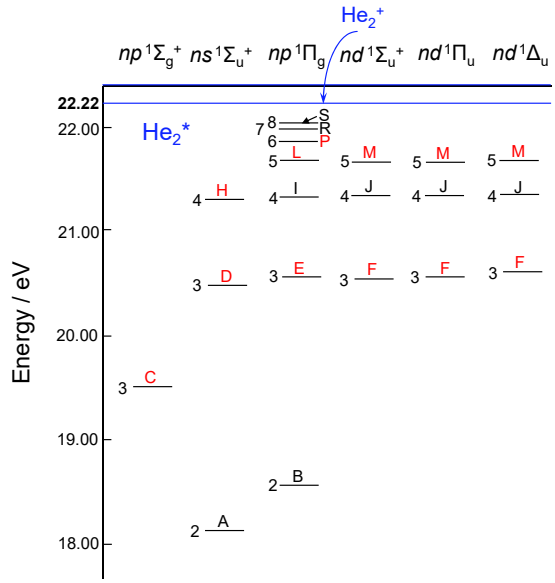

Fig. 3. Energy-level diagram of singlet states of He_2^*. Observed emitting levels in the $He_2^+/2e^-$ CRR reaction are shown in red.

3.2 Relative formation rate constants of He_2^* excimer in the $He_2^+/2e^-$ CRR reaction

Relative emission intensities of each emission system, given in Table 1, are proportional to their emission rate constants. When there is no nonradiative decay and pumping from the observation region, the emission rate constants correspond to their formation ones. To the best of our knowledge, no nonradiative decay processes have been known for the He_2^* states. Radiative lifetimes of the d, e, and f states have been measured as 25±5 ns, 57±10 ns, and 19±5 ns, respectively.[23)] Although radiative lifetimes of other excited states observed in this study are unknown, they may be the same order as the above states. Radiative lifetimes of excited He_2^* molecules (≤57 ns) are expected to be short enough to emit radiation within the observation region. It is therefore reasonable to assume that the relative emission rate constants reflect their formation ones.

The overall rate constant of the production of an upper state of He_2^*, $k(u)$, is given by summation of direct formation rate constant, $k_0(u)$, and the contribution of radiative cascade from upper states, $k(u\text{: cascade})$,

$$k(u) = k_0(u) + k(u\text{: cascade}). \qquad (5)$$

Actually radiative cascade partially contributes to the formation of the lowest energy c state (Table 1). Its $k_0(u)$ value was estimated by subtracting the contribution of radiative cascade. Results obtained are given in Table 2, where T_0 or T_e values of He_2^* states are shown. When vibrational constants of He_2^* states are known, T_0 values are calculated. On the other hand, when vibrational constants of He_2^* are unknown, T_e values are given in Table 2. The dependence of $k_0(u)$ on the energy of He_2^* state is shown in Fig. 4.

The $k_0(u)$ values decrease rapidly with increasing excitation energy of He_2* for both the triplet and singlet states. They are largest for the lowest $c^3\Sigma_g^+$ and $C^1\Sigma_g^+$ states. The total formation ratio of triplet/singlet states was 5.1, which was larger than a statistical ratio of 3.0 by 70%.

3.3 Vibrational distribution of He_2* and rotational distributions of He_2(f, e, d, c: $v' = 0$) in the $He_2^+/2e^-$ CRR reaction

Only (0,0) bands were observed for all the He_2* systems, so that no vibrational excitation was observed. Equilibrium internuclear distances of He_2* are given in Table 2.[19] It is clear that equilibrium internuclear distances of the observed He_2* states (1.068−1.097 Å) are similar to that of He_2^+ ($X^2\Sigma_u^+$:1.081 Å).[19] Thus, one reason for the lack of vibrational excitation is large Franck-Condon factors (FCFs) for the $He_2^+(X: v'' = 0) \rightarrow He_2$* recombination due to similar equilibrium internuclear distance.

In order to confirm the validity of the above explanation, we calculated FCFs from the $He_2^+(X: v'' = 0)$ to major He_2(d, c, and C: $v' = 0$–2) vibrational states using Morse potentials.[24] Results obtained are shown in Table 3. The FCFs for the $0-0$ transitions are

Table 2. Observed triplet and singlet excited states, energies (E_{state}), relative direct formation rate constants ($k_0(u)$), and equilibrium internuclear distance (r_e) of He_2* excimer.

State	E_{state} (eV)	$k_0(u)$	r_e[a] (Å)	State	E_{state} (eV)	$k_0(u)$	r_e (Å)
$q^3\Delta_u(6d\delta)$	21.8 (T_e)	6.9	1.090				
$q^3\Pi_u(6d\pi)$	21.8 (T_e)						
$q^3\Sigma_u^+(6d\sigma)$	21.8 (T_e)						
$p^3\Pi_g(6p\pi)$	21.8	1.5	1.080	$P^1\Pi_g(6p\pi)$	21.8	1.4	1.080
$o^3\Sigma_u^+(6s\sigma)$	21.8	2.4	1.089				
$m^3\Delta_u(5d\delta)$	21.7	9.3	1.091	$M^1\Delta_u(5d\delta)$	21.7	1.0	1.091
$m^3\Pi_u(5d\pi)$	21.7			$M^1\Pi_u(5d\pi)$	21.7		
$m^3\Sigma_u^+(5d\sigma)$	21.7			$M^1\Sigma_u^+(5d\sigma)$	21.7		
$l^3\Pi_g(5p\pi)$	21.7	3.9	1.080	$L^1\Pi_g(5p\pi)$	21.7	2.6	1.079
$k^3\Sigma_u^+(5s\sigma)$	21.6	3.0	1.079				
$k'^3\Sigma_g^+(5p\sigma)$	21.5	1.3	1.068				
$j^3\Delta_u(4d\delta)$	21.4	6.1	1.081				
$j^3\Pi_u(4d\pi)$	21.4		1.083				
$j^3\Sigma_u^+(4d\sigma)$	21.4						
$i^3\Pi_g(4p\pi)$	21.3	6.8	1.079				
$h^3\Sigma_u^+(4s\sigma)$	21.3	2.4	1.077	$H^1\Sigma_u^+(4s\sigma)$	21.3	1.4	1.077
$f^3\Delta_u(3d\delta)$	20.7	15.2	1.079	$F^1\Delta_u(3d\delta)$	20.7	3.7	1.079
$f^3\Pi_u(3d\pi)$	20.7	16.2	1.087	$F^1\Pi_u(3d\pi)$	20.7	3.3	1.085
$f^3\Sigma_u^+(3d\sigma)$	20.6	12.8	1.091	$F^1\Sigma_u^+(3d\sigma)$	20.7	2.1	1.089
$e^3\Pi_g(3p\pi)$	20.6	11.4	1.075	$E^1\Pi_g(3p\pi)$	20.7	2.0	1.076
$d^3\Sigma_u^+(3s\sigma)$	20.5	14.2	1.071	$D^1\Sigma_u^+(3s\sigma)$	20.6	5.0	1.069
$c^3\Sigma_g^+(3p\sigma)$	19.3	100	1.097	$C^1\Sigma_g^+(3p\sigma)$	19.6	19.1	1.093

a) Ref. 19

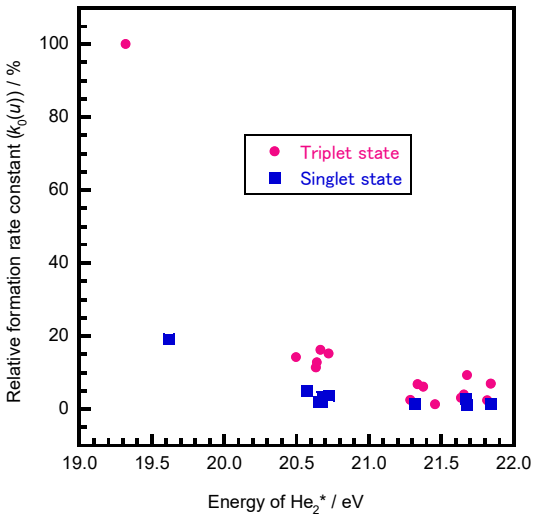

Fig. 4. Relative formation rate constants of triplet and singlet states of He_2^* produced from the $He_2^+/2e^-$ CRR in the He FA.

Table 3. Franck-Condon factors between $He_2^+(X^2\Sigma_u^+: v'' = 0)$ and $He_2(d,c,C: v' = 0–2)$ states.

$v'' - v'$	0 – 0	0 – 1	0 – 2
$He_2^+ \rightarrow d^3\Sigma_u^+$	0.995	0.481(-2)[a)]	0.279(-4)
$He_2^+ \rightarrow c^3\Sigma_g^+$	0.992	0.771(-2)	0.165(-3)
$He_2^+ \rightarrow C^1\Sigma_g^+$	0.992	0.771(-2)	0.165(-3)

larger than 0.99 in all the three systems. These data support why vibrational excitation is insignificant for the formation of He_2^* in the $He_2^+/2e^-$ CRR reaction.

Rotational populations of He_2^* were estimated for four typical band systems, for which rotational structures are well resolved. Figures 5a–5d show expanded emission spectra of the $f^3\Sigma_u^+–b^3\Pi_g$, $e^3\Pi_g–a^3\Sigma_u^+$, $d^3\Sigma_u^+–b^3\Pi_g$, and $c\,^3\Sigma_g^+–a^3\Sigma_u^+$ systems of He_2, where (0,0) bands of the four systems are observed. In ^4He, the nuclear spin is zero and due to the symmetry rules for homonuclear molecules all even or odd numbered rotational levels are missing.[25)] Therefore, only odd or even levels of P, Q, or R branches are observed in the above four transitions.[26-28)]

Rotational distributions of the f, e, d, and c states were determined from relative intensities of Q or P branch. Rotational levels of He_2^* which belong to Hund's case (b) are represented by the quantum number N'. The band intensity (photons s^{-1}) of a transition from a $(v'\,N')$ level to a $(v''N'')$ level is expressed as

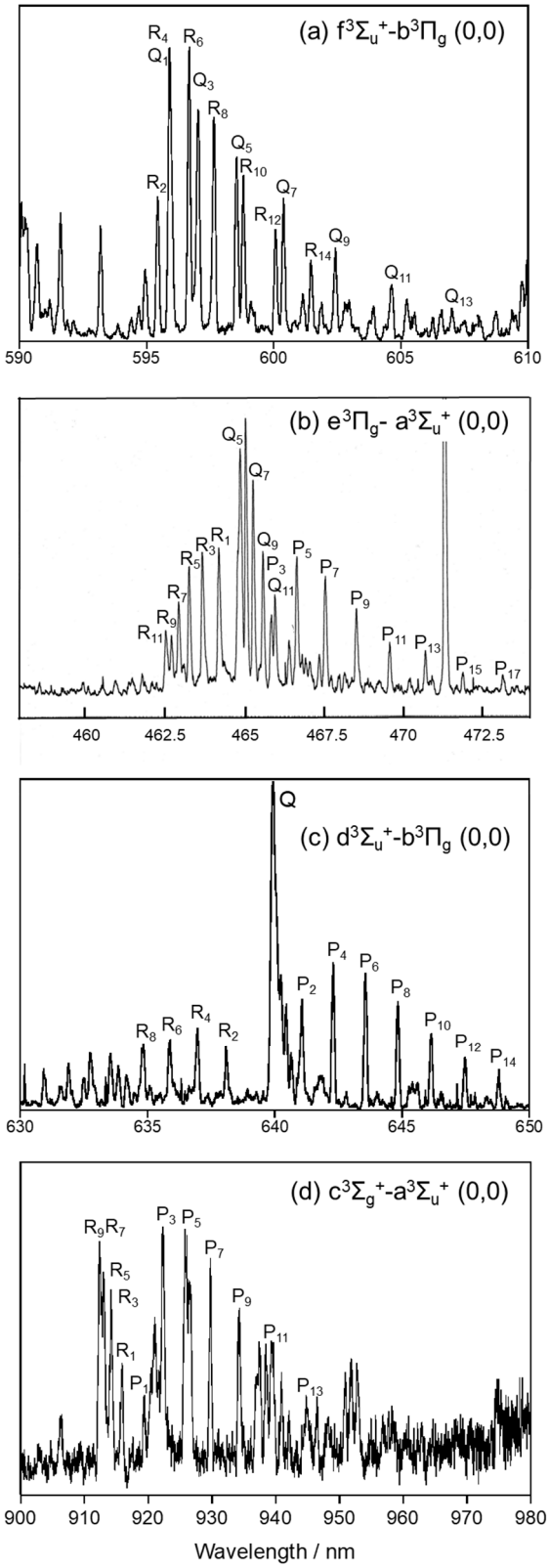

Fig. 5. Rotational structures of the (0,0) bands of He_2(f-b, e-a, d-b, c-a) systems resulting from the $He_2^+/2e^-$ CRR in the He FA at a He gas pressure of 1.8 Torr.

$$I_{v'N'v''N''} \propto N_{v'N'} Re^2(\bar{r}_{v'v''}) q_{v'v''} \nu^3_{v'N'v''N''} S_{N'N''}/g_{N'}, \quad (6)$$

where $N_{v'N'}$ is the rotational population in a given vibrational level, $Re(\bar{r}_{v'v''})$ the electronic transition moment, $q_{v'v''}$ the FCF, $\nu_{v'N'v''N''}$ the transition frequency, $S_{N'N''}$ the rotational line strength, and $g_{N'} = 2N' + 1$.[25] When a fixed (v', v'') band, $Re(\bar{r}_{v'v''})$ and $q_{v'v''}$ values are constant. Assuming a Boltzmann distribution, Boltzmann rotational temperature is obtained from the following relation,

$$\ln\left(\frac{I_{N'N''}}{\nu^3_{N'N''} S_{N'N''}}\right) \propto const - hcB_{v'}N'(N'+1)/kT_{Rot}, \quad (7)$$

where k and T_{Rot} are the Boltzmann constant and the Boltzmann rotational temperature, respectively.[25] In Figs. 6a–6d, $\ln(I_{N'N''}/\nu^3_{N'N''}S_{N'N''})$ values are plotted against $N'(N'+1)$ for the $v' = 0$ levels of the f, e, d, and c and states. An approximately linear relationship, i.e., approximately a Boltzmann distribution, is obtained for the above four levels. From the slopes, $hcB_{v'}/kT_{Rot}$, the effective rotational temperatures, T_{Rot}, are estimated to be 580±20 K for N'= 5–13 of He_2(f), 990±190 K for N'= 10–16 of He_2(e), and 830±20 K for N'= 7–17 of He_2(d), respectively. However, the populations at lower N' levels appear to deviate from the linear relationship. Their effective rotational temperatures are 310±70 K for N'=1–5 of He_2(f), 500±20 K for N'=2–10 of He_2(e), and 440±50 K for N'=1–7 of He_2(d). The rotational population of He_2(c) is expressed by a single Boltzmann distribution with an effective rotational temperature of 720±140 K. Above results are summarized in Table 4. The rotational temperatures of He_2(e) for low and high N' levels are in good agreement with

Table 4. Rotational temperatures of He_2(f,e,d,c) produced from the $He_2^+/2e^-$ CRR reaction.

Emitting species	T_r/ K
$He_2(f\,^3\Sigma_u^+: v'=0)$	580±20 (N'=5–13)
	310±70 (N'=1–5)
$He_2(e\,^3\Pi_g: v'=0)$	990±190 (N'=10–16)
	500±20 (N'=2–10)
$He_2(d\,^3\Sigma_u^+: v'=0)$	830±20 (N'=7–17)
	440±50 (N'=1–7)
$He_2(c\,^3\Sigma_g^+: v'=0)$	720±140 (N'=0–12)

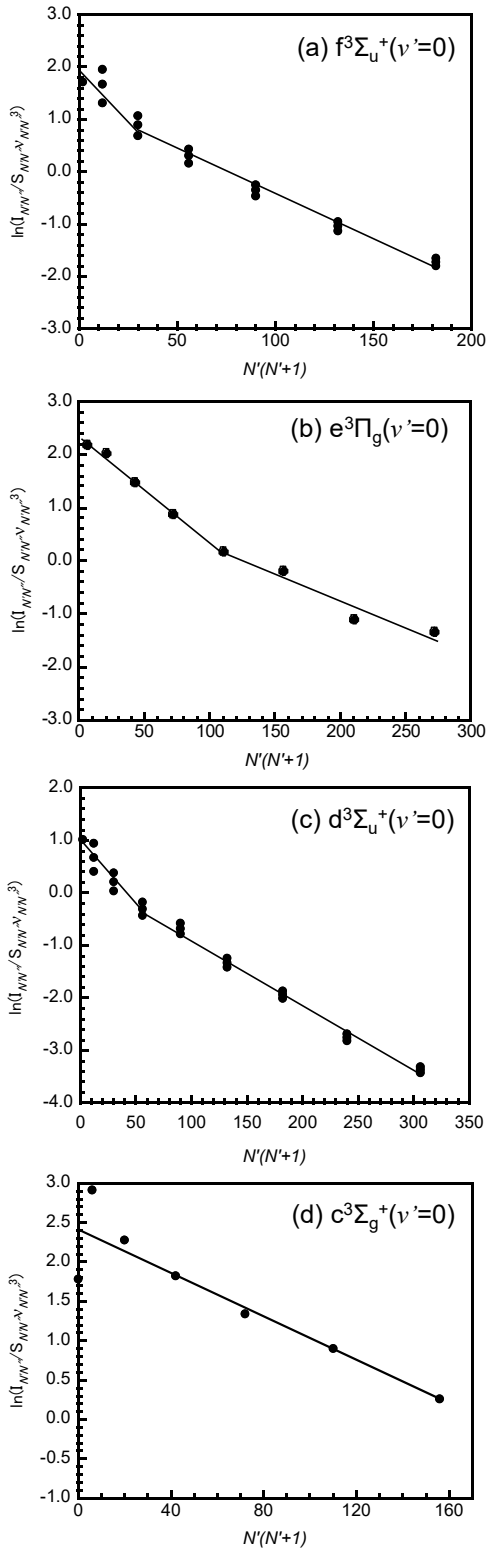

Fig. 6. Estimation of effective rotational temperatures from the slopes of $\ln(I_{N'N''}/\nu^3_{N'N''}S_{N'N''})$ against $N'(N'+1)$ for the He_2(f:v'=0), He_2(e:v'=0), He_2(d:v'=0), and He_2(c:v'=0) states in the $He_2^+/2e^-$ CRR reaction.

previous reported values of 492 and 903 K at p_{dn} = 1.4 Torr.[10]

In order to examine collisional relaxation, dependence of rotational populations on the buffer He gas pressure was examined in the 1.8–20 Torr range. The rotational distributions of He_2 (f: v' = 0) and He_2 (d: v' = 0) were essentially independent of the He pressure in the 1.8–20 Torr range, indicating that collisional relaxation within short radiative lifetimes of f(19±5 ns) and d(25±5 ns) states[23] was insignificant under our experimental conditions. The rotational distributions of He_2(f: v' = 0), He_2(e: v' = 0), and He_2(d: v' = 0) reproduced by double Boltzmann rotational temperatures. Similar double Boltzmann rotational distributions have been found for the e state.[10] Therefore, double Boltzmann rotational distributions may be general features for the formation of He_2^* in the $He_2^+/2e^-$ CRR reaction.

From the observed rovibrational distributions of He_2(f,e,d,c), we estimated the average vibrational and rotational energies of each state, denoted as $<E_v>$ and $<E_r>$, and the average yields of total available energy into these degrees of freedom, denoted as $<f_v>$ and $<f_r>$, respectively. Here, the total available energy, E_{tot}, was estimated from the relation at 300 K: $E_{tot} = -\Delta H_0^o + 5/2RT$. From the $<E_v>$, $<E_r>$, $<f_v>$ and $<f_r>$ values, the relative translational energy $<E_t>$ and the average yield of total available energy into the relative translational energy $<f_t>$ were determined. Results obtained are summarized in Table 5. The $<f_r>$ value decreases with increasing the E_{tot} value. This implies that the total excess energy is not efficiently converted into the rotational energy of He_2^*. On the basis of energetic data given in Table 5, most of total available energies (95.2–98.5 %) are released to relative translational energies of products. This implies that a third-body electron efficiently receives an excess energy as its translational energy during neutralization reaction.

3.4 Comparison between observed and statistical prior rotational and vibrational distributions of He_2^* excimer

In order to obtain information on reaction dynamics, statistical prior rotational and vibrational distributions,[29] were calculated assuming a long lived $[He_2^*–e^-]$ complex:

Table 5. Average vibrational, rotational, and translational energies (eV) deposited into He_2(f,e,d,c), total available energy (E_{tot}: eV), and average fractions of vibrational, rotational, and translational energies (%) deposited into He_2(f,e,d,c) + e^- in the $He_2^+/2e^-$ CRR reaction.

	He_2(f)	He_2(e)	He_2(d)	He_2(c)
$<E_v>$	0.00	0.00	0.00	0.00
$<E_r>$	0.079	0.056	0.059	0.043
E_{tot}	1.65	1.65	1.79	2.97
$<f_v>$	0.00	0.00	0.00	0.00
$<f_r>$	4.8	3.4	3.3	1.5
$<f_v>+<f_r>$	4.8	3.4	3.3	1.5
$<f_t>$	95.2	96.6	96.7	98.5

$$He_2^+ + 2e^- \rightarrow [He_2^*–e^-] \rightarrow He_2^* + e^-. \quad (8)$$

Prior rotational and vibrational distributions were calculated from the Eqs. (9) and (10), respectively:

$$P^o(N') \propto (2N'+1)(E_{tot} - E_{N'})^{1/2}, \quad (9)$$

$$P^o(v') \propto (E_{tot} - E_{v'})^{3/2}. \quad (10)$$

The prior rotational distributions of He_2 (f), He_2(e), He_2(d), and He_2(c) are compared with observed ones in Figs. 7a–7d, respectively. The prior vibrational distributions of v'=0–5 levels of He_2(f, e, d, c) states were calculated as follow:

He_2(f: v'=0–5) = 1.00:0.83:0.68:0.55:0.43:0.34,
He_2(e: v'=0–5) = 1.00:0.82:0.66:0.52:0.39:0.28,
He_2(d: v'=0–5) = 1.00:0.84:0.69:0.56:0.44:0.34,
He_2(c: v'=0–5) = 1.00:0.91:0.83:0.75:0.69:0.63.

The prior rotational and vibrational distributions predict much higher rotational and vibrational excitation than the observed ones. On the basis of these facts, He_2^* molecules are not formed through long-lived $[He_2–e^-]^*$, where the excess energies are deposited into all degrees of freedom statistically.

The deviation from prior rotational distribution can often be expressed in the form of surprisal,[29]

$$I_R = -\ln[P(v',N')/P^o(v',N')] = \theta_0 + \theta_R g_{N'}, \quad (11)$$

where $g_{N'} = E_{N'}/E_{tot}$.

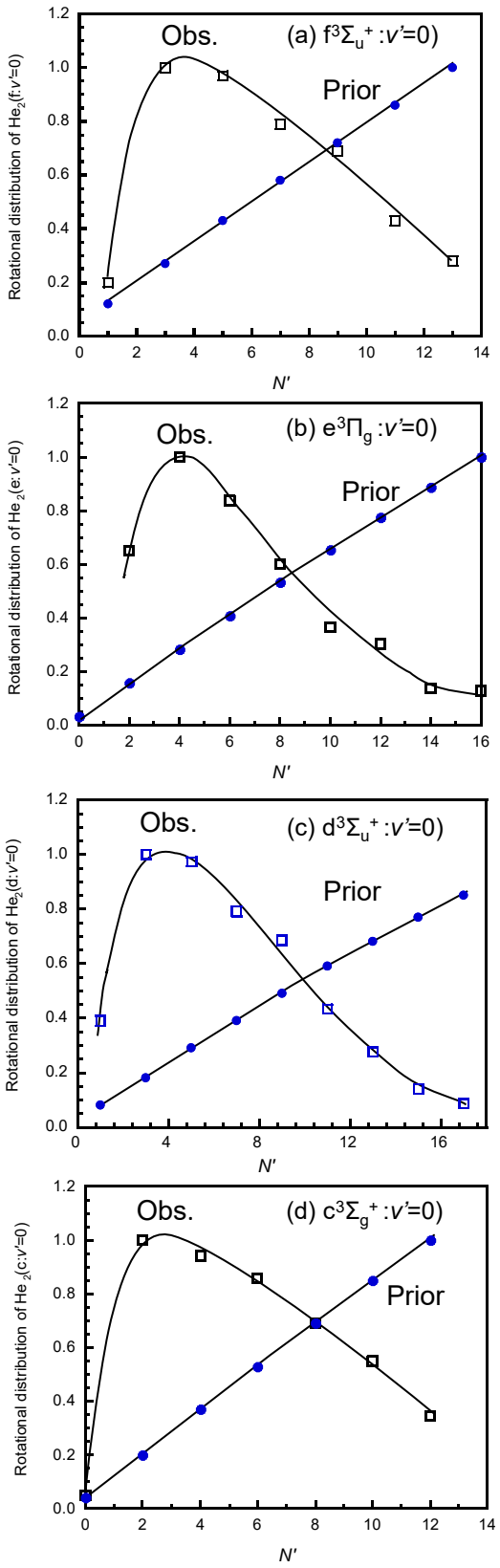

Fig. 7. Observed and statistical prior rotational distributions of the He_2(f: $v'=0$), He_2(e: $v'=0$), He_2(d: $v'=0$), and He_2(c: $v'=0$) states in the $He_2^+/2e^-$ CRR reaction

Figures 8a–8d show rotational surprisal plots of He_2(f: $v'=0$), He_2(e: $v'=0$), He_2(d: $v'=0$), and He_2(c: $v'=0$), respectively. When the two-body dissociation model (8) is used for $P^o(N')$, good linear relationships are found in the four surprisal plots. These results imply that an exponential gap behavior is present between the experimental and statistical distributions. From slopes of each surprisal plot, large positive surprisal parameters of 23.4, 25.6, 27.2, and 45.8 are obtained for He_2 (f: $v'=0$), He_2(e: $v'=0$), He_2(d: $v'=0$), and He_2(c: $v'=0$), respectively.

4. Summary and Conclusion

He_2* excimer emissions from twenty-two triplet states and twelve singlet states with excitation energies of 19.3–21.8 eV and 19.6–21.8 eV region, respectively, were observed by the $He_2^+/2e^-$ CRR reaction in the He afterglow. It was found that more He_2* states in wide energy range are formed in the $He_2^+/2e^-$ CRR reaction than those observed by Schmeltekopf and Broida[10] and Collins and Robertson.[11] The relative formation rate constant of He_2*, $k_0(u)$, rapidly decreased with increasing the excitation energy. A similar tendency was observed for He* in the $He^+/2e^-$ CRR reaction,[13] indicating that CRR reaction dynamics is similar between atomic He^+ and molecular He_2^+ ions. Major triplet and singlet product He_2* states were the lowest observed $c^3\Sigma_g^+$ and $C^1\Sigma_g^+$ states, which occupied 39.9% and 7.1% of $\sum_u k_0(u)$, respectively. The total formation ratio of triplet/singlet states was 5.1. No vibrational excitation was observed for all thirty-four states. The rotational distributions of $f^3\Sigma_u^+(v'=0)$, $e^3\Pi_g(v'=0)$, and $d^3\Sigma_u^+(v'=0)$ were expressed by double Boltzmann rotational temperatures, whereas that of $c^3\Sigma_g^+(v'=0)$ was represented by a single Boltzmann temperature. On the basis of observed rovibrational distributions, most of the total excess energy (95.2–98.5%) is deposited into the relative translational energy of products. The observed vibrational and rotational distributions were lower than those of statistical prior ones calculated assuming a long lived [He_2*–e^-] intermediate. It was therefore concluded that He_2* molecules are not formed via long lived [He_2*–e^-] intermediate, where excess energies are statistically distributed to all degrees of freedom.

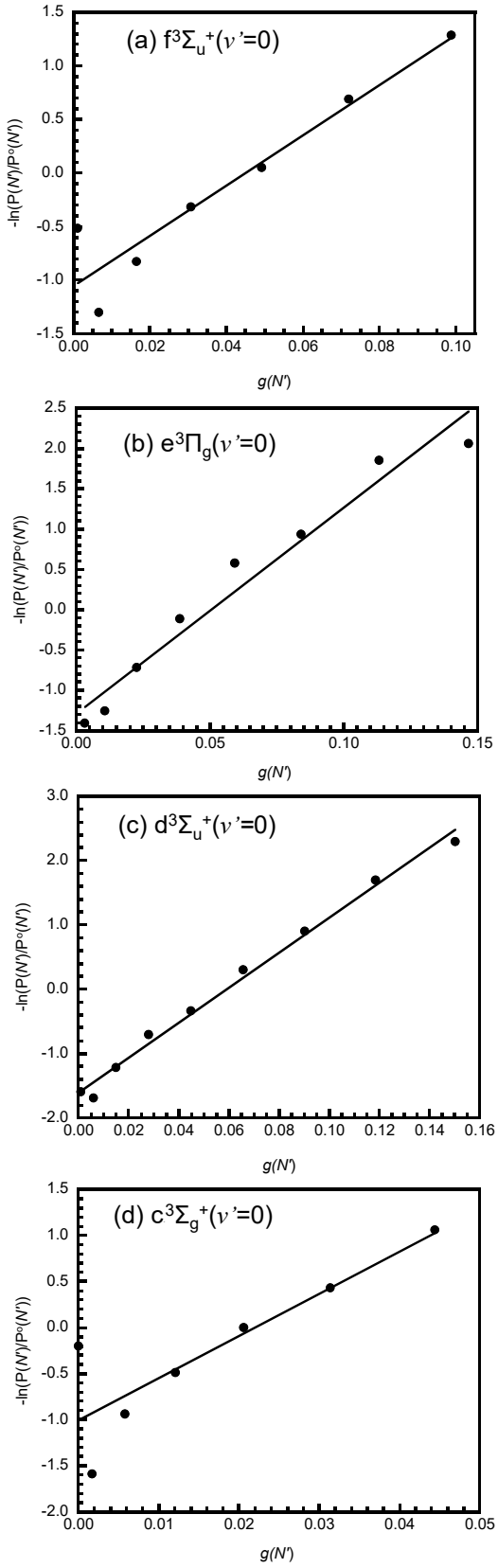

Fig. 8. Rotational surprisal plots for the He_2(f: $v'=0$), He_2(e: $v'=0$), He_2(d: $v'=0$), and He_2(c: $v'=0$) states in the $He_2^+/2e^-$ CRR reaction.

Acknowledgments

The authors thank Prof. Kenji Furuya for his helpful comments and the Mitsubishi foundation (1996) for financial support.

References

1) D. R. Bates, A. E. Kingston, and R. W. P. McWhirter, *Proc. R. Soc., Ser. A*, 267, 297 (1962).
2) M. R. Flannery, *Adv. At, Mol. Opt. Phys.*, 32, 117 (1994).
3) H. J. Oskam and V. R. Mittelsdadt, *Phys. Rev.*, 132, 1445 (1963).
4) E. E. Ferguson, F. C. Fehsenfeld, and A. L. Schmeltekopf, *Phys. Rev.*, 138, 381 (1965).
5) C. J. Chen, *J. Chem. Phys.*, 50, 1560 (1969).
6) J. Berlande, M. Cheret, R. Deloche, A. Gonfalone, and C. Manus, *Phys. Rev. A*, 1, 887 (1970).
7) G. E. Veatch, H. J. Oskam, *Phys. Rev. A*, 1, 1498 (1970).
8) J. Stevefelt, J. Boulmer, and J.-F. Delpech, *Phys. Rev. A*, 12, 1246 (1975).
9) P. Dohnal, T. Kotrik, J. Varju, I. Korolov, R. Plasil, and J. Glosik, *WDS'10 Proceedings of Contributed Papers, Part II*, 42, (2010).
10) A. L. Schmeltekopf, Jr. and H. P. Broida, *J. Chem. Phys.*, 39, 1261 (1963).
11) C. B. Collins and W. W. Robertson, *J. Chem. Phys.*, 40, 2208 (1964).
12) M. Nakamura, M. Tsuji, M. Tanaka, and Y. Nishimura, *Chem. Lett.*, 25, 279 (1996).
13) M. Tsuji, M. Nakamura, E. Oda, M. Hisano, and Y. Nishimura, *Jpn. J. Appl. Phys.*, 37, 5775 (1998).
14) M. Tsuji, M. Hisano, K. Uto, J. Hayashi, and T. Tsuji, *Eng. Sci. Rep. Kyushu Univ.*, 44, 1 (2023).
15) M. Tsuji, T. Matsuzaki, and T. Tsuji, *Chem. Phys.*, 285, 335 (2002).
16) M. Tsuji, in "*Advances in Gas-Phase Ion Chemistry" Vol. 4.*, Edited by N. G. Adams and L. M. Babcock, Elsevier, 137 (2001).
17) H. Sekiya, M. Tsuji, and Y. Nishimura, *J. Chem. Phys.*, 87, 325 (1987).
18) Y. Ikezoe, S. Matsuoka, M. Takebe, and A. Viggiano, "*Gas Phase Ion-Molecule Reaction Rate Constants through 1986*", Maruzen, Tokyo (1987).
19) K. P. Huber and G. Herzberg, "*Molecular Spectra and Molecular Structure, IV. Constants of Diatomic Molecules*", Van Nostrand Reinhold, New York (1979).
20) *Atomic Spectra Database*, *NIST Standard Reference Database*, 78, Ver. 5.9. Oct. (2021).
21) M. Endoh, M. Tsuji, and Y. Nishimura, *J. Chem. Phys.*, 79, 5368 (1983).
22) S. Yamaguchi, M. Tsuji, and Y. Nishimura, *J. Chem. Phys.*, 88, 3111 (1988).
23) S. Neeser, R. Tietz, M. Schulz, and H. Langhoff, *Z. Phys. D.*, 31, 61 (1994).
24) M. Shimauchi, *Bunko Kenkyu* (*J. Spectrosc. Soc. Jpn.*), 25, 65 (1976).
25) G. Herzberg, "*Molecular Spectra and Molecular Structure: I. Spectra of Diatomic Molecules*", 2nd ed. Van Nostrand Reinhold, New York (1950).
26) M. L. Ginter, *J. Chem. Phys.*, 42, 561 (1965).
27) M. L. Ginter, *J. Mol. Spectrosc.*, 18, 321 (1965).
28) C. M. Brown and M. L. Ginter, *J. Mol. Spectrosc.*, 40, 302 (1971).
29) R. D. Levine, *Bull. Chem. Soc. Jpn.*, 61, 29 (1988).